

Sensing weak anharmonicities with a passive-active anti-PT symmetric system

Ya-Wei Zeng,¹ Wei-Xin Chen,¹ Tian-Le Yang,¹ Wan-Jun Su,¹ and Huaizhi Wu¹

¹*Fujian Key Laboratory of Quantum Information and Quantum Optics
and Department of Physics, Fuzhou University, Fuzhou 350116, China*

We propose a scheme for enhanced sensing of weak anharmonicities based on a three-mode anti-parity-time (anti-PT) symmetric cavity-magnon-waveguide system. By tuning the optical gain to the active cavity mode, the linewidth suppression point for the anti-PT symmetric Hamiltonian can be flexibly controlled even when the two dissipative magnonic modes experience strong intrinsic decay. This essential characteristic is utilized for detecting weak nonlinearities in both the cavity and magnonic modes, with both demonstrating similar high levels of sensitivity. Moreover, the sensitivity can be greatly improved with a detuned laser drive. Based on the integrated passive-active three-mode anti-PT symmetric system, the sensing scheme can be generalized to various physical systems with anharmonicities.

I. INTRODUCTION

Sensing has attracted widespread interest across a broad range of fields, including optics [1–3], magnon-cavity hybrid systems [4], and electrical circuit resonators [5, 6]. In quantum mechanics, the Hermicity of the Hamiltonian and its real eigenvalues in closed systems stand as fundamental postulates. Regarding sensing within conventional Hermitian systems, the eigenvalue splitting, which refers to the energy splitting between two levels, induced by a linear perturbation ϵ is directly proportional to the magnitude of ϵ . Mathematically, the sensitivity of a Hermitian system to a linear perturbation can be expressed as a functional dependence $\Delta\omega \propto \epsilon$. In recent years, the enhancement of sensitivity by harnessing non-Hermitian degeneracies and exceptional points (EPs) has been the subject of intensive theoretical and experimental investigations [7–15]. Parity-time (PT) symmetric systems, a unique subclass of non-Hermitian systems, are defined by the invariance of their Hamiltonian under the combined transformation of the PT operator [16–23], satisfy a specific commutation relation formulated as $[H, PT] = 0$. When subjected to a linear perturbation, the resulting eigenvalue splitting follows a scaling law of $\epsilon^{1/N}$, where the PT symmetric system's N eigenvalues and their corresponding eigenvectors converge. Consequently, for sufficiently small perturbations, the eigenvalue splitting behavior at EPs is significantly more sensitive than that in Hermitian systems. This characteristic has already found applications in many practical sensing scenarios [24–26].

Sensing schemes based on anti-parity-time (anti-PT) symmetric systems have also garnered considerable attention [27–42]. For anti-PT symmetric systems, the Hamiltonian exhibits an anti-commutation relationship with the PT operator, which can be mathematically expressed as $\{PT, H\} = 0$. The anti-PT symmetric systems can be applied not only for the sensing of linear perturbations [29], but also, remarkably, for efficient sensing of nonlinear perturbations [43]. The latter is built upon a dissipatively coupled two-mode system [43] with vacuum-induced coherence (VIC) between the two modes [44–46].

The VIC can induce linewidth suppression, a singularity point which can be used for enhanced sensing of weak magnetic nonlinearities. This paradigm has also been generalized to integrated cavity-waveguide optomechanical systems, where the joint effect of optical bistability and linewidth suppression can greatly enhance the sensitivity of detecting optomechanically induced nonlinearities [47]. Nevertheless, the practical implementation of such two-mode anti-PT symmetric systems is hindered by inherent drawbacks. Specifically, there exist unavoidable intrinsic losses for the coupled subsystems [48–50], which would lead to a strong quenching in the magnon response to the nonlinearities and thus its sensitivity to anharmonicities [43].

In order to effectively circumvent the drawbacks inherent in two-mode anti-PT symmetric systems, in this paper, we explore sensing of Kerr nonlinearities by using a passive-active anti-PT symmetric system, comprising one active cavity mode and two dissipative magnonic modes. Intriguingly, the VIC-induced linewidth suppression, typically associated with intrinsically lossless systems, can still be achieved and actively controlled through optical gain—even when the two magnon modes experience significant individual losses, with decay rates comparable to half the dissipative coupling strength. Note that the linewidth suppression point functions as the EP in PT-symmetric systems, and can be used for enhanced sensitivity to weak Kerr nonlinearity in both the cavity mode and the magnonic modes. The anti-PT symmetric system keeps away from optical bistability with resonant driving, corresponding to the linewidth suppression point. However, by introducing an appropriate laser detuning to the cavity mode, the sensitivity to the weak nonlinearities can be increased by about fifty percent. Thus, the three-mode passive-active anti-PT symmetric configuration exhibits notable advantages compared to conventional two-mode systems, and may find potential applications in a wide class of systems, including waveguide cavity optomechanical systems and hybrid cavity magnonic systems.

The paper is structured as follows. Section II is dedicated to the introduction of our physical model and

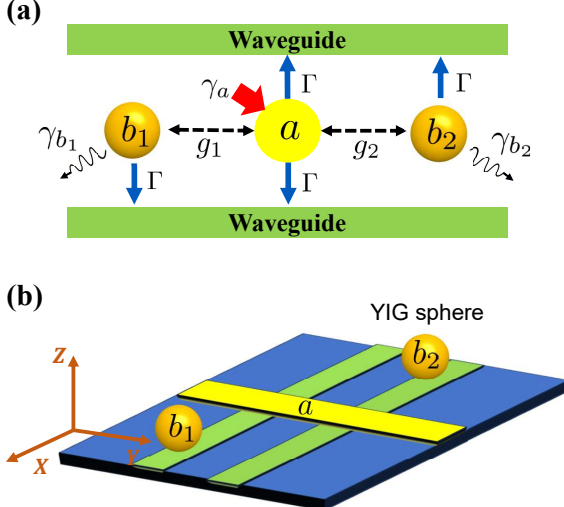


FIG. 1. (a) Theoretical model and (b) Schematic of the cavity-magnon-waveguide setup. The microwave cavity running transverse to the waveguide interacts with two YIG spheres via the transmission line. g_1 and g_2 are the coherent coupling strengths between the active cavity mode a and the two magnon modes b_1 and b_2 , respectively. The magnon modes b_1 and b_2 also dissipatively couple to the cavity via the waveguides, with the rates Γ being identical to the cavity-waveguide coupling. γ_{b_1} and γ_{b_2} are the damping rates of b_1 and b_2 , and $\gamma_a = \kappa_- - \kappa_+$ denotes the effective gain of the cavity mode a (i.e., the net rate defined by the difference between cavity loss and incoherent gain).

the detailed elaboration of the eigenvalues of the anti-PT symmetric Hamiltonian. Section III showcases the enhanced sensing capabilities for weak nonlinearities in both the cavity mode (Sec. III A) and the magnonic modes (Sec. III B). Section IV delves into the practical implementation aspects of the physical model, and then gives the conclusion of this work. In Appendix A, we present the stability criterion for our three-mode anti-PT symmetric system. Appendix B elaborates on the system dynamics when a non-zero laser detuning to the cavity mode is taken into account.

II. THE ANTI-PT SYMMETRIC SYSTEM WITH AN ACTIVE MODE

We consider a three-mode cavity-magnon-waveguide system as schematically illustrated in Figs. 1 (a) and 1(b). A microwave cavity (mode a) is dissipatively coupled to two yttrium iron garnet (YIG) spheres — each hosting a magnon mode b_j ($j = 1, 2$) — via two separate waveguides, with coupling strengths Γ between mode a and each b_j ($j = 1, 2$). Due to spatial overlap, the cavity mode a may also coherently couple to magnon mode b_j with weak strength g_j . The cavity mode a is externally driven by a laser operating at a frequency of ω_d with the strength Ω . In addition, the cavity mode a and the

magnon modes b_j may exhibit Kerr-type anharmonicity, arising either from the nonlinear response of the electric polarization in optical resonators [51–54] or from the intrinsic nonlinear magnetization dynamics in magnetic systems [55–57]. The Hamiltonian of the system can be effectively described by

$$H = \sum_{j=1,2} [\omega_j b_j^\dagger b_j + g_j (b_j^\dagger a + b_j a^\dagger)] + \omega_a a^\dagger a + \sum_{j=1,2} U_{b_j} b_j^{\dagger 2} b_j^2 + U_a a^{\dagger 2} a^2 + i\Omega (a^\dagger e^{-i\omega_d t} - a e^{i\omega_d t}), \quad (1)$$

where ω_j (ω_a) are the resonance frequencies of mode b_j (a). The parameters U_{b_j} characterize the intrinsic magnon anharmonicity of the YIG modes b_j [56]; while U_a denotes the cavity's self-Kerr nonlinearity, which can arise naturally, for example, through coupling to a nonlinear qubit [54].

We introduce the Lindblad master equation to account for dissipative processes mediated by the environment, including both reservoir-induced coupling through the common waveguide and spontaneous decay channels arising from thermal baths [58]. When the localized modes $b_{1(2)}$ and a are coupled to a one-dimensional waveguide with a finite separation, adiabatic elimination of the waveguide degrees of freedom under the Markov approximation yields a master equation describing the resulting coherent and dissipative interactions. In addition, incoherent pumping may be applied to the cavity mode a to generate optical gain, a mechanism well established in microwave QED systems, including inverted qubits [59] and engineered reservoirs [60]. Incorporating these decay and gain channels leads to the driven-dissipative dynamics of the full three-mode system as described by the master equation for the density matrix ρ :

$$\frac{d\rho}{dt} = -\frac{i}{\hbar} [H, \rho] + \gamma_{b_1} \mathcal{L}[b_1] \rho + \gamma_{b_2} \mathcal{L}[b_2] \rho + \kappa_- \mathcal{L}[a] \rho + \kappa_+ \mathcal{L}[a^\dagger] \rho + 2\Gamma \mathcal{L}[m_1] \rho + 2\Gamma \mathcal{L}[m_2] \rho, \quad (2)$$

where \mathcal{L} is the Liouvillian operator given by $\mathcal{L}[\sigma] \rho = 2\sigma\rho\sigma^\dagger - \sigma^\dagger\sigma\rho - \rho\sigma^\dagger\sigma$ with $\sigma = a, a^\dagger, b_j$. The term $\mathcal{L}[b_{1(2)}] \rho$ describes spontaneous decay of the magnonic modes with the rate $\gamma_{b_{1(2)}}$. The terms $\kappa_- \mathcal{L}[a] \rho + \kappa_+ \mathcal{L}[a^\dagger] \rho$ represent an open cavity with both loss (of the rate κ_-) and incoherent gain, where photons are injected at rate κ_+ (e.g., through optical pumping or coupling to an inverted atomic ensemble) [60–62]. The waveguide-mediated dissipator takes the form $\mathcal{L}[m_j] \rho$, where the jump operators m_j ($j = 1, 2$) is a linear superposition of the annihilation operators b_j and a , i.e. $m_j = v_j b_j + u_j e^{i\Phi_j} a$. Here Φ_j denote the propagation phase acquired between the mode positions, and the coefficients v_j and u_j characterize their respective coupling strengths to the travelling-wave reservoir [60]. The associated decay rate into the waveguide is the standard

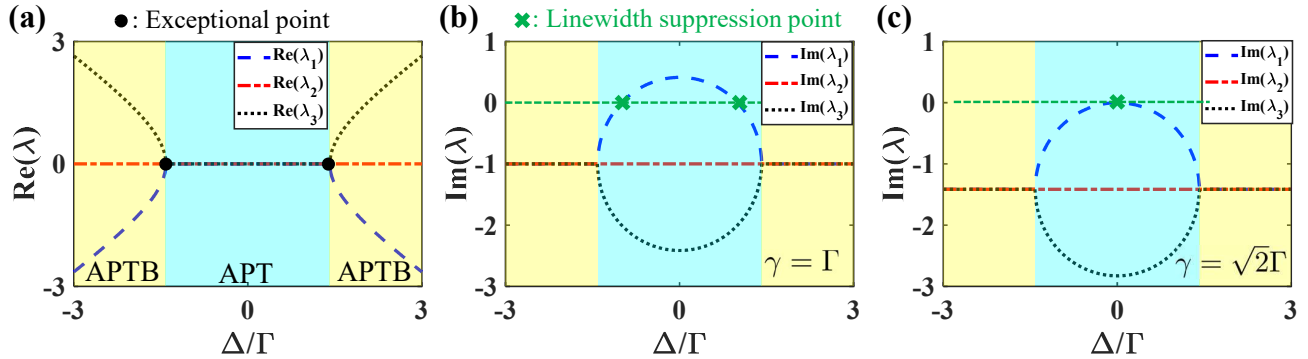


FIG. 2. (a) Real parts (eigenfrequencies) and (b), (c) imaginary parts (linewidths) of the eigenvalues for the anti-PT symmetric system (with $g = 0$) plotted against Δ . The EPs appear at $\Delta = \pm\sqrt{2}\Gamma$. APT denotes the anti-PT symmetric phase, and APTB represents the anti-PT symmetry broken phase. Panels (b) and (c), show the imaginary parts of the eigenvalues under the conditions of $\gamma = \Gamma$ and $\gamma = \sqrt{2}\Gamma$, respectively. The green dashed line is used to screen out the parameter conditions when the imaginary part of the eigenvalue is zero, which are marked with green crosses.

Fermi–Golden–Rule rate Γ , which represents the external (radiative) damping depending on the vacuum coupling strength, the local photonic density of states (or the group velocity of the waveguide mode). When the cavity and magnon modes couple identically to the common reservoir and the propagation phases are tuned to $\Phi = \Phi_1 = \Phi_2 = 2k\pi$ (with integer k), the dissipative coupling leads to symmetric optical–magnonic supermodes of the form $m_j = (b_j + a)/\sqrt{2}$.

To treat the nonlinear term analytically, we adopt the mean-field approximation, i.e. $\langle o_1 o_2 \rangle = \langle o_1 \rangle \langle o_2 \rangle$ for any two operators. We further assume that the system operates in a zero-temperature environment with white Gaussian noise. By choosing a proper rotating frame with respect to the driving frequency ω_d , and denoting $\alpha(t) = \langle a(t) \rangle$ ($\beta_j = \langle b_j(t) \rangle$), the simplified form of the evolution equation is expressed as

$$\begin{pmatrix} \dot{\beta}_1 \\ \dot{\alpha} \\ \dot{\beta}_2 \end{pmatrix} = -i\mathcal{H} \begin{pmatrix} \beta_1 \\ \alpha \\ \beta_2 \end{pmatrix} - 2i\mathcal{R} \begin{pmatrix} \beta_1 \\ \alpha \\ \beta_2 \end{pmatrix} + \Omega \begin{pmatrix} 0 \\ 1 \\ 0 \end{pmatrix} \quad (3)$$

with

$$\mathcal{R} = \begin{pmatrix} U_{b_1} \beta_1^* \beta_1 & 0 & 0 \\ 0 & U_a \alpha^* \alpha & 0 \\ 0 & 0 & U_{b_2} \beta_2^* \beta_2 \end{pmatrix} \quad (4)$$

and

$$\mathcal{H} = \begin{pmatrix} \tilde{\Delta}_1 - i\Gamma & g_1 - i\Gamma & 0 \\ g_1 - i\Gamma & \Delta_a - i(\gamma_a + 2\Gamma) & g_2 - i\Gamma \\ 0 & g_2 - i\Gamma & \tilde{\Delta}_2 - i\Gamma \end{pmatrix}, \quad (5)$$

where $\tilde{\Delta}_j = \Delta_j - i\gamma_{b_j}$ with $\Delta_j = \omega_j - \omega_d$, $\Delta_a = \omega_a - \omega_d$, and $\gamma_a =: \kappa_- - \kappa_+$ denotes the effective damping rate of the cavity mode, with positive (negative) values corresponding to net loss (gain).

We begin with an analysis of the linear dynamics by setting $U_a = U_{b_2} = 0$. Moreover, we assume that $\Delta_a = 0$,

$\Delta = \Delta_1 = -\Delta_2$, $\gamma = \gamma_{b_j} + \Gamma = \gamma_a + 2\Gamma$, then the eigenvalues of \mathcal{H} read

$$\begin{aligned} \lambda_1 &= -i \left(\gamma - \sqrt{2\Gamma^2 + 4ig\Gamma - 2g^2 - \Delta^2} \right), \\ \lambda_2 &= -i\gamma, \\ \lambda_3 &= -i \left(\gamma + \sqrt{2\Gamma^2 + 4ig\Gamma - 2g^2 - \Delta^2} \right), \end{aligned} \quad (6)$$

where we have kept the coherent coupling strength $g_1 = g_2 = g$ for later discussions. In the absence of spatial overlap between the cavity and magnon modes, the direct couplings between them are negligible, i.e. $g_1 = g_2 = 0$. Then, \mathcal{H} reduces to a three-mode anti-PT symmetric Hamiltonian given by

$$\mathcal{H} = \begin{pmatrix} \Delta - i\gamma & -i\Gamma & 0 \\ -i\Gamma & -i\gamma & -i\Gamma \\ 0 & -i\Gamma & -\Delta - i\gamma \end{pmatrix}, \quad (7)$$

which obeys $(PT)\mathcal{H}(PT)^{-1} = -\mathcal{H}$, with the parity operator (P) exchanging the first and third modes, and keeping the second mode fixed. We show the eigenvalues with $g = 0$ in Fig. 2. The blue area in the figure represents the anti-PT symmetric region (APT), while the yellow areas represent the anti-PT symmetry broken regions (APTB). The EPs occur at $\Delta = \pm\sqrt{2}\Gamma$ where the three eigenvalues coalesce and become degenerate. Moreover, linewidth suppression arises when both the real and imaginary parts of an eigenvalue simultaneously approach zero, and appears in the anti-PT symmetric phase ($|\Delta| < \sqrt{2}\Gamma$) where $E_p \equiv \Delta^2 + \gamma^2 - 2\Gamma^2 \rightarrow 0$.

For the three-mode system discussed here, the condition $E_p \approx 0$ implies that the linewidth suppression signature is geometrically governed by an elliptic curve in the (Δ, γ) parameter space (normalized by Γ), which also serves as the stability boundary (see Appendix A). Remarkably, the linewidth suppression effect persists even when both modes b_1 and b_2 remain lossy, due to the presence of gain in the cavity mode. As can be seen in Fig.

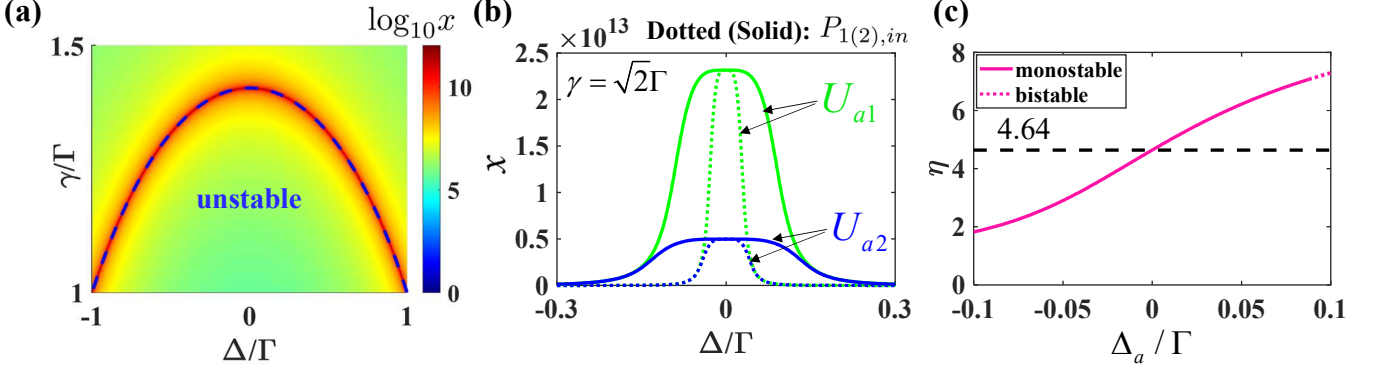


FIG. 3. (a) The rescaled cavity response $\log_{10} x$ plotted against Δ and γ for $U_a/2\pi = 1$ nHz and $\Delta_a = 0$. The blue dashed line delineates the boundary of the unstable region and corresponds to the set of linewidth suppression points. (b) The cavity responses plotted against Δ with different nonlinearity strengths $U_{a1}/2\pi = 0.1$ nHz and $U_{a2}/2\pi = 1$ nHz and two different drive powers. Here we have set $\gamma = \sqrt{2}\Gamma$, $\Delta_a = 0$, $P_{1,in} = 8$ μ W, and $P_{2,in} = 8$ mW. At $\Delta = 0$, the peak in the cavity response arises from linewidth suppression. For comparison, the green- and blue-dotted curves have been scaled up by 10. (c) The ratio η as a function of Δ_a , at the drive power of 8 mW and $\Delta = 0$ with $U_{a1} = 0.1$ μ Hz and $U_{a2} = 1$ μ Hz. The monostable regime and bistable regime are denoted by the pink solid line and dotted line, respectively. The horizontal dashed line represents the response enhancement factor of 4.64, corresponding to the sensitivity at the linewidth suppression condition. Other parameters are: $\Gamma/2\pi = 1$ MHz, $\kappa_- = 0.05\Gamma$, $\lambda_d = 1550$ nm, $\Omega = \sqrt{P_{j,in}\kappa_-/\hbar\omega_d}$.

2(b), when the decay rates of the magnon modes are vanishing, i.e. $\gamma_{b_j} = 0$ (or $\gamma = \Gamma$), the singularities arise at $\Delta = \pm\Gamma$ for the optical gain $-\gamma_a = \Gamma$. For the special case of $\gamma = \sqrt{2}\Gamma$, there exists only a unique singularity point with zero linewidth, as shown in Fig. 2(c). In this case, the decay rate of the magnon modes is explicitly given by $\gamma_{b_j} = (\sqrt{2} - 1)\Gamma$, and the effective gain of the cavity mode is $-\gamma_a = (2 - \sqrt{2})\Gamma$. In general, two singularities associated with linewidth suppression can be observed at the detuning $\Delta = \pm\sqrt{\Gamma^2 - \gamma_{b_j}^2 - 2\Gamma\gamma_{b_j}}$, provided that the magnon decay rate lies within the range $0 < \gamma_{b_j} < (\sqrt{2} - 1)\Gamma$. This highlights a clear advantage compared to two-mode systems, in which linewidth suppression is limited to cases where none of the modes suffers spontaneous loss to its independent surrounding [43].

III. ENHANCED SENSING TO ANHARMONICITIES DUE TO LINEWIDTH SUPPRESSION

For sensing of weak anharmonicities, one can simply consider the resonant condition $\Delta = 0$ (where the cavity and magnon modes are resonant), and tailor the magnon-waveguide coupling to meet $\gamma_{b_j} = (\sqrt{2} - 1)\Gamma$, which allows the resonant cavity drive to produce a large and highly nonlinear cavity (or magnon) response, see the details later. In practice, however, when the two magnon modes are non-degenerate $\Delta \neq 0$, one can tune the optical gain so that the operating point falls inside the stable region, near linewidth-suppression point.

With the appropriate choice of the driving and pumping strengths, the system is in the stable regime. The

steady-state solutions for the mean values β_1 , α and β_2 of the corresponding modes b_1 , a and b_2 are

$$\begin{aligned} \beta_1 &= \frac{-\Gamma(-i\Delta + \gamma)}{(\Delta^2 + \gamma^2 - 2\Gamma^2)\gamma} \Omega, \\ \alpha &= \frac{\Delta^2 + \gamma^2}{(\Delta^2 + \gamma^2 - 2\Gamma^2)\gamma} \Omega, \\ \beta_2 &= \frac{-\Gamma(i\Delta + \gamma)}{(\Delta^2 + \gamma^2 - 2\Gamma^2)\gamma} \Omega, \end{aligned} \quad (8)$$

where the linear response will diverge under the condition $\Delta^2 + \gamma^2 - 2\Gamma^2 \rightarrow 0$. It is worth mentioning that the condition for linewidth suppression (i.e. $E_p \rightarrow 0$) is consistent with the divergent behavior of the steady-state solutions in Eq. (8). This implies that linewidth suppression may lead to a considerable sensing potential for internal or external perturbations [43]. In the following, we illustrate that the scheme can be used to sense optical Kerr-type nonlinearities, which arise from the nonlinear response of the electric polarization in optical resonators, as well as to detect intrinsic magnonic nonlinearities originating from nonlinear magnetization dynamics. Such nonlinearities are ubiquitous in dispersive atom-resonator [51, 52], magnon-photon [53, 63], and optomechanical interactions [3]. Remarkably, recent experiments have demonstrated substantial Kerr coefficients in optical cavities ($U_a/2\pi = -12.2 \pm 0.1$ kHz/photon [55]). In YIG spheres, the Kerr coefficient can be tuned from 0.05 to 100 nHz as the sphere diameter is varied from 1 mm to 100 μ m [56, 57].

A. Nonlinear cavity

To explore nonlinearity sensing, we begin by introducing the nonlinear term associated with the cavity mode. The modified steady-state equations for the magnon and cavity modes are

$$\begin{aligned} 0 &= -i(\Delta - i\gamma)\beta_1 - \Gamma\alpha, \\ 0 &= -\gamma\alpha - 2iU_a|\alpha|^2\alpha - \Gamma\beta_1 - \Gamma\beta_2 + \Omega, \\ 0 &= -i(-\Delta - i\gamma)\beta_2 - \Gamma\alpha. \end{aligned} \quad (9)$$

By eliminating β_1 and β_2 , the cavity response $x = |\alpha|^2$ is found to satisfy a cubic relation

$$I = 4U_a^2x^3 + \frac{\gamma^2E_p^2}{(\Delta^2 + \gamma^2)^2}x, \quad (10)$$

where $I = \Omega^2$. The optical bistability can not occur since the derivative $dI/dx = 0$ has no solution for any drive power, see Appendix B. This represents another advantage over the two-mode anti-PT symmetric system, in which bistability would be observed when the laser power I is greater than a threshold value [64]. In the vicinity of linewidth suppression points, i.e. $E_p \rightarrow 0$, the linear term in Eq. (10) becomes negligible, and the cavity response approximates to $x \approx (I/4U_a^2)^{\frac{1}{3}}$. Note that x is highly sensitive to variations in U , and the sensitivity to U_a in the response goes as $|\partial x/\partial U_a| \propto |U_a|^{-\frac{5}{3}}$. It is worthwhile to emphasize that the inherent damping for the magnon modes, which is inevitable due to mode defects, would reduce the sensitivity to nonlinearities as the linewidth suppression condition can not be met with the conventional two-lossy-mode setup [43]. In contrast, the three-mode setup with an active cavity helps sustain the high sensitivity.

In Fig. 3(a), we plot the response x as a function of Δ and γ with the nonlinearity strength $U_a/2\pi = 1$ nHz and a weak drive power $P_{1,in} = 8 \mu\text{W}$. As illustrated by the dashed line in Fig. 3(a), for a fixed value of γ , there may exist two detunings Δ corresponding to linewidth suppression points, where the cavity displays a strong and sharply varying response near the suppression points, enabling effective sensing while avoiding any instability. Moreover, in Fig. 3(b), we show the line cuts along $\gamma = \sqrt{2}\Gamma$ for two different nonlinearities $U_{a1}/2\pi = 0.1$ nHz and $U_{a2}/2\pi = 1$ nHz, respectively. The peak response is found at resonance $\Delta = 0$ as a result of linewidth suppression. In analogy to the lossless two-mode system [43], a tenfold decrease in nonlinearity strength gives rise to a 4.64-fold enhancement of the cavity response, hence leading to a remarkably enhanced sensitivity to nonlinearities. However, in the above case with $\gamma = \sqrt{2}\Gamma$, the decay rates of the two magnon modes are $\gamma_0 = (\sqrt{2}-1)\Gamma$, implying that the sensing of weak optical nonlinearities on the order of nHz can be achieved even in the presence of two highly lossy magnon modes. In addition, we increase the input power to $P_{2,in} = 8 \text{ mW}$,

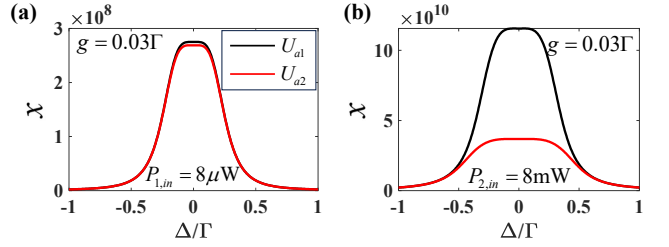


FIG. 4. The cavity responses plotted against Δ in the presence of a coherent coupling $g = 0.03\Gamma$ with drive powers (a) $8 \mu\text{W}$ and (b) 8 mW . Other parameters are the same as in Fig. 3(c).

which broadens the lineshape of the cavity response without changing the ratio $x(U_{a1})/x(U_{a2})$ at $\Delta = 0$. Importantly, under this condition the system is stable for all detunings Δ , and Fig. 3(b) shows that the response remains robust against small detuning fluctuations. This ensures that the operating point is experimentally accessible and insensitive to small noise in Δ .

So far, we consider that the laser driving is in resonance with the cavity mode a . However, we find that an appropriate detuning Δ_a for the cavity mode a can further enhance the sensitivity outside the optical bistability regime. For this purpose, we quantify the sensitivity with the measure defined by the ratio $\eta = x(U_{a1})/x(U_{a2})$, where $x(U_{a1})$ and $x(U_{a2})$ denote the responses corresponding to cavity nonlinearity strengths $U_{a1} = 0.1 \mu\text{Hz}$ and $U_{a2} = 1 \mu\text{Hz}$, respectively. As shown in Fig. 3(c), we plot η as a function of the detuning Δ_a , where the solid and the dotted lines denote the monostable and bistable regimes, respectively, see Appendix B. Notably, when the detuning satisfies $0.08\Gamma > \Delta_a > 0$, the ratio $\eta \sim 7$ can be achieved in the monostable regime. This ratio is much greater than the typical 4.64-fold enhancement at the linewidth suppression point.

In addition, we consider the effect of a finite coherent coupling g between the modes with $\Delta_a = 0$. For $g \neq 0$, the real singularity is now replaced by a complex one, i.e., the eigenvalue $\lambda_1 = -i\gamma + i\sqrt{2\Gamma^2 + 4ig\Gamma - 2g^2 - \Delta^2}$ has a nonvanishing imaginary part with $E_p \rightarrow 0$. In this case, a tenfold variation in U_a can only lead to a small change in cavity response as shown in Fig. 4(a). Thus, the sensitivity becomes weak as $\eta \sim 1$. Nevertheless, by increasing the strength of input laser power from $8 \mu\text{W}$ to 8 mW , one can again recover high sensitivity, see Fig. 4(b).

B. Nonlinear magnonic system

We now turn to sensing the nonlinearity in one of the magnon modes and suppose a nonlinear b_1 without loss of generality. The steady-state relations are now given

by

$$\begin{aligned} 0 &= -i(\Delta - i\gamma)\beta_1 - 2iU_{b_1}|\beta_1|^2\beta_1 - \Gamma\alpha, \\ 0 &= -\gamma\alpha - \Gamma\beta_1 - \Gamma\beta_2 + \Omega, \\ 0 &= -i(-\Delta - i\gamma)\beta_2 - \Gamma\alpha. \end{aligned} \quad (11)$$

From these, we obtain the spin-current response of the YIG sphere, defined as $y = |\beta_1|^2$, which satisfies the cubic relation:

$$I = \frac{4U_{b_1}^2[(\gamma^2 - \Gamma^2)^2 + \gamma^2\Delta^2]y^3 - 4U_{b_1}\Delta\gamma^2E_p y^2 + \gamma^2E_p^2y}{\Gamma^2(\Delta^2 + \gamma^2)}. \quad (12)$$

In the vicinity of the linewidth suppression points where $E_p \rightarrow 0$, the coefficients of the quadratic term y^2 and the linear term y become vanishingly small. As a result, the spin-current response becomes highly sensitive to variations in U_{b_1} and approximately follows the functional dependence

$$y \approx \left\{ \frac{I\Gamma^2(\Delta^2 + \gamma^2)}{4U_{b_1}^2[(\gamma^2 - \Gamma^2)^2 + \gamma^2\Delta^2]} \right\}^{\frac{1}{3}} \approx \left(\frac{I}{2U_{b_1}^2} \right)^{\frac{1}{3}}. \quad (13)$$

Hence, the sensitivity to U_{b_1} in the response is again encoded as $|\partial y/\partial U_{b_1}| \propto |U_{b_1}|^{-\frac{5}{3}}$, which is the same as the case of a nonlinear cavity. Alternatively, based on Eq. (11), the cavity response $x = |\alpha|^2$ can also be written by

$$I = \left| \frac{\Gamma^2}{-i(\Delta + 2U_{b_1}y) - \gamma} + \gamma + \frac{\Gamma^2}{i\Delta - \gamma} \right|^2 x. \quad (14)$$

For $E_p \rightarrow 0$ and considering the EP singularity with respect to $\Delta = 0$, one can again find that $|\partial x/\partial U_{b_1}| \sim \frac{\partial}{\partial U} (I/U_{b_1}^2)^{1/3} \propto |U_{b_1}|^{-\frac{5}{3}}$. Without loss of generality, we show the spin current response in what follows.

To demonstrate the sensing of Kerr nonlinearities intrinsic to magnon mode, we examine the response for two weak nonlinearity strengths $U_{b_1} = 0.1$ nHz and $U_{b_1} = 1$ nHz under the weak drive power $P_{in} = 8$ μ W. As shown in Fig. 5(a), we plot the response y against Δ for the intrinsic decay rates of the magnonic modes being $\gamma_{b_j} = (\sqrt{2} - 1)\Gamma$ and the optical gain $-\gamma_a = (2 - \sqrt{2})\Gamma$. For $\Delta = 0$, a tenfold decrease in nonlinearity strength again gives rise to a 4.64-fold enhancement of the spin current response as a result of the linewidth suppression. Furthermore, in Fig. 5(b), we show the ratio of the spin current response $\eta = y(U_{b_11})/y(U_{b_12})$ by introducing an appropriate detuning Δ_a from cavity resonance, with $U_{b_11} = 0.1$ μ Hz and $U_{b_12} = 1$ μ Hz. As the system keeps away from the bistable regime (the dotted part), a higher sensitivity of $\eta \sim 7$ can be reached for $\Delta_a \sim 0.05\Gamma$, analogous to what is observed in a nonlinear cavity.

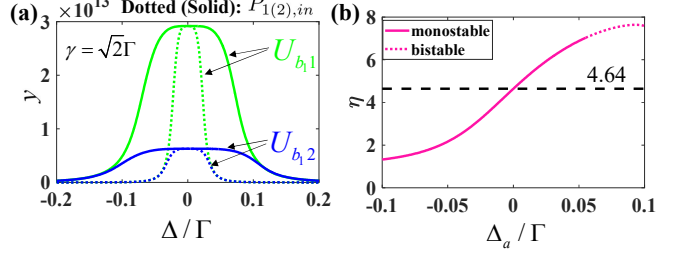


FIG. 5. (a) The magnon spin-current responses plotted against Δ for $\gamma = \sqrt{2}\Gamma$ with weak Kerr nonlinearity strengths $U_{b_11}/2\pi = 0.1$ nHz and $U_{b_12}/2\pi = 1$ nHz. The green- and blue-dotted curves have been scaled up by 10. The spin-current responses show similar behavior to those in sensing weak cavity nonlinearity. (b) η as a function of Δ_a , at the drive power of 8 mW for two different nonlinearity strengths $U_{b_11} = 0.1$ μ Hz and $U_{b_12} = 1$ μ Hz. The monostable regime and bistable regime are denoted by the pink solid line and dotted line, respectively. The horizontal dashed line represents the response enhancement factor of 4.64, corresponding to the sensitivity at the linewidth suppression condition. Other parameters are the same as Fig. 3(c).

IV. EXPERIMENTAL REALIZATION AND DISCUSSION

To construct a three-mode passive-active anti-PT symmetric system, the cavity mode must be active, which can be achieved by adding an external driving field on auxiliary qubits [59] or optical gain medium [65]. The damping rates and resonance frequencies of the magnon modes, which arise from the surface roughness, the impurities, and defects in the YIG sphere, can be alternatively controlled by a grounded loop antenna getting close to the YIG sphere and an external magnetic field [4]. With that in hand, we consider an integrated apparatus comprising two YIG spheres and a microwave cavity, where the cavity is dissipatively coupled to the two YIG spheres through two different waveguides. Owing to the nonexistent spatial overlap between the cavity and magnon modes, the direct couplings between them are dropped. Then the full Hamiltonian in the presence of the external drive can be cast exactly in the form of Eq. (1). By tuning the damping and gain of the modes, the passive-active anti-PT symmetric system can be realized [48, 63].

The three-mode anti-PT-symmetric configuration is well suited for detecting weak anharmonicities associated with passive magnon modes, the detectable range of the anharmonicity (U_a or U_{b_j}) is determined by the regime in which the nonlinear correction remains weak (i.e., $\{U_a|\alpha|^2, U_{b_j}|\beta|^2\}/\Gamma < 1$), so that the linear coupling between the cavity and magnonic modes continues to dominate the response. For anharmonicities $\{U_a, U_{b_j}\}$ in the nHz (μ Hz) range, the corresponding ratios are on the order of 10^{-3} (10^{-1}). In these weakly nonlinear regimes, the steady-state solution reduces to $x \simeq (I/4U_a^2)^{1/3}$ [or $y \simeq (I/4U_{b_j}^2)^{1/3}$], implying a sensitivity

$|\partial x/\partial U_a| \propto U_a^{-5/3}$ [or $|\partial y/\partial U_{b_j}| \propto U_{b_j}^{-5/3}$], which diverges as $U_{a(b_j)} \rightarrow 0$. Thus, an extremely small nonlinearity, down to the nHz scale in the cavity or YIG implementation, remain detectable. The practical upper bound on $U_{a(b_j)}$ is set by the onset of strong-drive nonlinear effects when $\{U_{ax}, U_{b_j}y\} \sim \Gamma$, where higher-order terms modify the energy spectrum of the anti-PT symmetric system and degrade the linewidth suppression induced sensitivity enhancement. At low powers the response obeys $\{x, y\} \sim I^{1/3}$, so the signal increases with drive but without entering instability. When the drive is too strong, additional nonlinear resonances appear, reducing the monotonic sensitivity to $U_{a(b_j)}$. Similarly, the sensitivity increases when Δ_a is tuned towards the onset of the bistability. Beyond this point, $\{U_{ax}, U_{b_j}y\}$ may undergo a transition and exhibit nonlinear behavior - a regime in which the sensing scheme becomes ineffective.

In summary, we have investigated the enhanced sensing of weak nonlinearities within a passive-active anti-PT symmetric system where the active cavity mode dissipatively couples to two magnon modes with intrinsic losses. The system Hamiltonian maintains the anti-PT symmetry characteristic, and its eigenvalue may display linewidth suppression points, which can be actively controlled by the optical gain even when the magnon modes experience independent losses. The EP-like singularity associated with linewidth suppression has been utilized to detect weak nonlinearities in both the cavity mode and the magnonic modes [43]. For the scenario where only the cavity mode exhibits nonlinearity, a tenfold decrease in nonlinearity strength gives rise to a 4.64-fold enhancement of the cavity response with a resonant cavity driving, where optical bistability can not happen, regardless of the driving strength and the nonlinearities. An appropriate drive detuning to cavity mode helps to increase and sensitivity by about fifty percent. For the case where one of the magnon modes contains Kerr nonlinearity, we obtain the same enhanced sensitivity manifested in both the cavity and spin current responses. Finally, we emphasize that the scheme does not necessitate the intrinsic losses of the modes to be zero and can be extended to a wide variety of systems, such as laser-cooled atomic ensembles [66], superconducting transmon qubits [24, 67, 68], and optomechanical systems [69–72].

ACKNOWLEDGMENTS

We thank Yong Li for helpful discussions. H.W. acknowledges support from the National Natural Science Foundation of China under Grant No. 12174058.

Appendix A: Stability of the system

A coupled three-mode system with nonlinearities may exhibit instability under a specific drive power, and such

instability is generally deemed undesirable. To ensure the system operates within a stable regime, we turn to the linearized dynamics. As presented in the main text, the system dynamics, expressed in terms of the annihilation (creation) operators, can be expanded as follows:

$$\begin{aligned} \dot{b}_1 &= -i\Delta_1 b_1 - \gamma_{b_1} b_1 - \Gamma b_1 - \Gamma a + b_{1,in}, \\ \dot{b}_1^\dagger &= i\Delta_1 b_1^\dagger - \gamma_{b_1} b_1^\dagger - \Gamma b_1^\dagger - \Gamma a^\dagger + b_{1,in}^\dagger, \\ \dot{a} &= -i\Delta_a a - \gamma_a b - 2iU_a a^\dagger a a - 2\Gamma a \\ &\quad - \Gamma b_1 - \Gamma b_2 + \Omega + a_{in}, \\ \dot{a}^\dagger &= i\Delta_a a^\dagger + 2iU_a a^\dagger a^\dagger a - 2\Gamma a^\dagger \\ &\quad - \Gamma b_1^\dagger - \Gamma b_2^\dagger + \Omega + a_{in}^\dagger, \\ \dot{b}_2 &= -i\Delta_2 b_2 - \gamma_{b_2} b_2 - \Gamma b_2 - \Gamma a + b_{2,in}, \\ \dot{b}_2^\dagger &= i\Delta_2 b_2^\dagger - \gamma_{b_2} b_2^\dagger - \Gamma b_2^\dagger - \Gamma a^\dagger + b_{2,in}^\dagger. \end{aligned} \quad (\text{A1})$$

where a_{in} , $b_{1,in}$, $b_{2,in}$ are white Gaussian noise with zero mean. Considering the anti-PT symmetric configuration, we impose the following conditions: $\Delta = \Delta_1 = -\Delta_2$, $\Delta_a = 0$, $\gamma_{b_1} = \gamma_{b_2} = \gamma_0$ and $\gamma = \gamma_0 + \Gamma = \gamma_a + 2\Gamma$. To incorporate fluctuations, we linearize the operators around the classical mean values as $b_1 = \beta_1 + \delta b_1$, $b_2 = \beta_2 + \delta b_2$ and $a = \alpha + \delta a$. The dynamics of the fluctuations can be further formulated as (by omitting quantum noise terms):

$$\begin{aligned} \dot{\delta b}_1 &= (-i\Delta - \gamma)\delta b_1 - \Gamma \delta a, \\ \dot{\delta b}_1^\dagger &= (i\Delta - \gamma)\delta b_1^\dagger - \Gamma \delta a^\dagger, \\ \dot{\delta a} &= -\gamma \delta a - 2iU_a(2|\alpha|^2 \delta a + \alpha^2 \delta a^\dagger) - \Gamma \delta b_1 - \Gamma \delta b_2, \\ \dot{\delta a}^\dagger &= -\gamma \delta a^\dagger + 2iU_a(2|\alpha|^2 \delta a^\dagger + \alpha^{*2} \delta a) - \Gamma \delta b_1^\dagger - \Gamma \delta b_2^\dagger, \\ \dot{\delta b}_2 &= (i\Delta - \gamma)\delta b_2 - \Gamma \delta a, \\ \dot{\delta b}_2^\dagger &= (-i\Delta - \gamma)\delta b_2^\dagger - \Gamma \delta a^\dagger. \end{aligned} \quad (\text{A2})$$

At a low drive power, the dynamics of the system can be characterized by a 3 by 3 anti-PT symmetric matrix, as the product $U|\alpha|^2$ is significantly smaller than Γ . The property of the system is predominantly determined by the eigenvalues of the Hamiltonian H described in the main text. This characteristic is attributed to the modified spectroscopic characteristics of the system under a weak probe. However, as the drive power increases, the nonlinear optical shift $U|\alpha|^2$ becomes comparable to Γ or even much larger than Γ . Thus, a more accurate description necessitates employing the higher-order matrix.

To inspect the system stability, the quadratures are utilized instead to describe the dynamics of the system: $\delta q_{b_1} = (\delta b_1 + \delta b_1^\dagger)/\sqrt{2}$, $\delta p_{b_1} = (\delta b_1 - \delta b_1^\dagger)/i\sqrt{2}$, $\delta q_a = (\delta a + \delta a^\dagger)/\sqrt{2}$, $\delta p_a = (\delta a - \delta a^\dagger)/i\sqrt{2}$, $\delta q_{b_2} = (\delta b_2 + \delta b_2^\dagger)/\sqrt{2}$, $\delta p_{b_2} = (\delta b_2 - \delta b_2^\dagger)/i\sqrt{2}$. For the new basis of the quadratures $\delta \varsigma = [\delta q_{b_1}, \delta p_{b_1}, \delta q_a, \delta p_a, \delta q_{b_2}, \delta p_{b_2}]$, the dynamics is dominated by $d\delta \varsigma/dt = \mathcal{M}\delta \varsigma$ with

$$\mathcal{M} = \begin{pmatrix} -\gamma & \Delta & -\Gamma & 0 & 0 & 0 \\ -\Delta & -\gamma & 0 & -\Gamma & 0 & 0 \\ -\Gamma & 0 & -\gamma - i\Lambda & \Sigma - \Xi & -\Gamma & 0 \\ 0 & -\Gamma & -\Sigma - \Xi & -\gamma + i\Lambda & 0 & -\Gamma \\ 0 & 0 & -\Gamma & 0 & -\gamma & -\Delta \\ 0 & 0 & 0 & -\Gamma & \Delta & -\gamma \end{pmatrix}, \quad (\text{A3})$$

where $\Lambda = U_a(\alpha^2 - \alpha^{*2})$, $\Xi = U_a(\alpha^2 + \alpha^{*2})$, and $\Sigma = 4U_a|\alpha|^2$. Following a consideration of the Routh-Hurwitz criterion [73], the real parts of the eigenvalues of the matrix \mathcal{M} must be strictly negative to ensure that the system is stable.

Appendix B: optical bistability for $\Delta_a \neq 0$

For $\Delta_a \neq 0$ and $g = 0$, the steady-state relations of the three-mode system are

$$\begin{aligned} 0 &= -i(\Delta - i\gamma)\beta_1 - \Gamma\alpha, \\ 0 &= -i(\Delta_a - i\gamma)\alpha - \Gamma\beta_1 - \Gamma\beta_2 \\ &\quad + 2iU_a|\alpha|^2\alpha + \Omega, \\ 0 &= -i(-\Delta - i\gamma)\beta_2 - \Gamma\alpha. \end{aligned} \quad (\text{B1})$$

Eliminating β_1 and β_2 , the cubic relation for the cavity response takes the form as

$$I = 4U_a^2x^3 - 4U_a\Delta_a x^2 + \left[\frac{\gamma^2(\Delta^2 + \gamma^2 - 2\Gamma^2)^2}{(\Delta^2 + \gamma^2)^2} + \Delta_a^2 \right] x, \quad (\text{B2})$$

where the quadratic term $\sim x^2$ is nonvanishing, and may lead to optical bistability.

[1] W. Chen, S. Kaya Özdemir, G. Zhao, J. Wiersig, and L. Yang, *Nature (London)* **548**, 192 (2017).

[2] H. Hodaei, A. U. Hassan, S. Wittek, H. Garcia-Gracia, R. El-Ganainy, D. N. Christodoulides, and M. Khajavikhan, *Nature (London)* **548**, 187 (2017).

[3] M. Aspelmeyer, T. J. Kippenberg, and F. Marquardt, *Rev. Mod. Phys.* **86**, 1391 (2014).

[4] Y. Yang, Y.-P. Wang, J. W. Rao, Y. S. Gui, B. M. Yao, W. Lu, and C.-M. Hu, *Phys. Rev. Lett.* **125**, 147202 (2020).

[5] B.-B. Zhou, W.-J. Deng, L.-F. Wang, L. Dong, and Q.-A. Huang, *Phys. Rev. Appl.* **13**, 064022 (2020).

[6] C. Youngsun, H. Choloong, Y. J. Woong, and S. S. Ho, *Nat. Commun.* **9**, 2182 (2018).

[7] Z. Xiao, H. Li, T. Kottos, and A. Alù, *Phys. Rev. Lett.* **123**, 213901 (2019).

[8] Z.-P. Liu, J. Zhang, S. Kaya Özdemir, B. Peng, H. Jing, X.-Y. Lü, C.-W. Li, L. Yang, F. Nori, and Y.-x. Liu, *Phys. Rev. Lett.* **117**, 110802 (2016).

[9] P.-Y. Chen and J. Jung, *Phys. Rev. Appl.* **5**, 064018 (2016).

[10] J. Wang, D. Mukhopadhyay, and G. S. Agarwal, *Phys. Rev. Res.* **4**, 013131 (2022).

[11] J. Wiersig, *Phys. Rev. A* **93**, 033809 (2016).

[12] Y.-Y. Li, Q.-T. Cao, J.-h. Chen, X.-C. Yu, and Y.-F. Xiao, *Phys. Rev. Appl.* **16**, 044016 (2021).

[13] Y. Li, Z. Deng, C. Qin, S. Wan, B. Lv, C. Guan, J. Yang, S. Zhang, and J. Shi, *Opt. Express* **31**, 492 (2023).

[14] S. Yu, Y. Meng, J.-S. Tang, X.-Y. Xu, Y.-T. Wang, P. Yin, Z.-J. Ke, W. Liu, Z.-P. Li, Y.-Z. Yang, G. Chen, Y.-J. Han, C.-F. Li, and G.-C. Guo, *Phys. Rev. Lett.* **125**, 240506 (2020).

[15] A. Felski and F. K. Kunst, *Phys. Rev. Res.* **7**, 013326 (2025).

[16] C. M. Bender and S. Boettcher, *Phys. Rev. Lett.* **80**, 5243 (1998).

[17] C. M. Bender, D. C. Brody, and H. F. Jones, *Phys. Rev. Lett.* **89**, 270401 (2002).

[18] C. M. Bender, M. Berry, and A. Mandilara, *J. Phys. A* **35**, L467 (2002).

[19] S. K. Özdemir, S. Rotter, F. Nori, and L. Yang, *Nat. Mater.* **18**, 783 (2019).

[20] D. Roy and G. S. Agarwal, *Phys. Rev. A* **111**, 013702 (2025).

[21] W. Wang, X. Wang, and G. Ma, *Phys. Rev. Lett.* **134**, 066301 (2025).

[22] R. Wang, L. Han, M.-N. Zhang, L.-F. Wang, and Q.-A. Huang, *Microsyst. Nanoeng.* **11**, 99 (2025).

[23] R. Wang, L. Han, M.-N. Zhang, L.-F. Wang, and Q.-A. Huang, *Commun. Phys.* **8**, 21 (2025).

[24] J. Zhang, Y.-L. Zhou, Y. Zuo, H. Zhang, P.-X. Chen, H. Jing, and L.-M. Kuang, *Adv. Quantum Technol.* **7**, 2300350 (2024).

[25] S. Sharma, A. Kani, and M. Bhattacharya, *Phys. Rev. A* **105**, 043505 (2022).

[26] C. Zeng, Y. Sun, G. Li, Y. Li, H. Jiang, Y. Yang, and H. Chen, *Opt. Express* **27**, 27562 (2019).

[27] Z. Feng and X. Sun, *Phys. Rev. Lett.* **129**, 273601 (2022).

[28] Y. Li, Y.-G. Peng, L. Han, M.-A. Miri, W. Li, M. Xiao, X.-F. Zhu, J. Zhao, A. Alù, S. Fan, and C.-W. Qiu, *Science* **364**, 170 (2019).

[29] H. Zhang, R. Huang, S.-D. Zhang, Y. Li, C.-W. Qiu, F. Nori, and H. Jing, *Nano Lett.* **20**, 7594 (2020).

[30] D. Mukhopadhyay, J. M. P. Nair, and G. S. Agarwal, *Phys. Rev. B* **105**, 064405 (2022).

[31] H. S. Xu and L. Jin, *Phys. Rev. A* **104**, 012218 (2021).

[32] F. Huang, L. Chen, L. Huang, J. Huang, G. Liu, Y. Chen, Y. Luo, and Z. Chen, *Phys. Rev. A* **104**, L031503 (2021).

[33] M. Peng, H. Zhang, Q. Zhang, T.-X. Lu, I. M. Mirza, and H. Jing, *Phys. Rev. A* **107**, 033507 (2023).

[34] F. Yang, Y.-C. Liu, and L. You, *Phys. Rev. A* **96**, 053845 (2017).

[35] Y. Qin, H. Chen, D. Luo, C. Pan, H. Hu, Y. Zhang, and D. Wei, *Opt. Express* **29**, 29175 (2021).

[36] X.-W. Luo, C. Zhang, and S. Du, *Phys. Rev. Lett.* **128**, 173602 (2022).

[37] F. Zhang, Y. Feng, X. Chen, L. Ge, and W. Wan, *Phys. Rev. Lett.* **124**, 053901 (2020).

[38] B. Li, Y. Zhang, J. Wang, J. Liu, M. Li, W. Wang, J. Ma, P. Yuan, D. Zhang, H. Zhu, H. Zhang, and L. Qian, *Phys. Rev. Res.* **7**, 023012 (2025).

[39] M. Jahangiri, G.-M. Parsanasab, and L. Hajshahvaladi, *Sci. Rep.* **15**, 4823 (2025).

[40] Y. Ren, D. Saparov, and Q. Niu, *Phys. Rev. Lett.* **134**, 206701 (2025).

[41] M. Yang, Q. Zhong, Z. Ye, S. Kaya Özdemir, M. Farhat, R. El-Ganainy, and P.-Y. Chen, *Phys. Rev. A* **110**, 033504 (2024).

[42] C. Li, R. Yang, X. Huang, Q. Fu, Y. Fan, and F. Zhang, *Phys. Rev. Lett.* **132**, 156601 (2024).

[43] J. M. P. Nair, D. Mukhopadhyay, and G. S. Agarwal, *Phys. Rev. Lett.* **126**, 180401 (2021).

[44] S. Das, A. Rakshit, and B. Deb, *Phys. Rev. A* **85**, 011401 (2012).

[45] A. Sitek and P. Machnikowski, *Phys. Rev. B* **86**, 205315 (2012).

[46] G. S. Agarwal, *Phys. Rev. Lett.* **84**, 5500 (2000).

[47] C.-W. Liu, Y. Liu, L. Du, W.-J. Su, H. Wu, and Y. Li, *Opt. Express* **31**, 9236 (2023).

[48] B. Bhoi, B. Kim, S.-H. Jang, J. Kim, J. Yang, Y.-J. Cho, and S.-K. Kim, *Phys. Rev. B* **99**, 134426 (2019).

[49] Y. Tabuchi, S. Ishino, T. Ishikawa, R. Yamazaki, K. Usami, and Y. Nakamura, *Phys. Rev. Lett.* **113**, 083603 (2014).

[50] X. Zhang, C.-L. Zou, L. Jiang, and H. X. Tang, *Phys. Rev. Lett.* **113**, 156401 (2014).

[51] S. Haroche and J.-M. Raimond, *Exploring the Quantum: Atoms, Cavities, and Photons* (Oxford University Press, 2006).

[52] J. Koch, T. M. Yu, J. Gambetta, A. A. Houck, D. I. Schuster, J. Majer, A. Blais, M. H. Devoret, S. M. Girvin, and R. J. Schoelkopf, *Phys. Rev. A* **76**, 042319 (2007).

[53] B. Zare Rameshti, S. Viola Kusminskiy, J. A. Haigh, K. Usami, D. Lachance-Quirion, Y. Nakamura, C.-M. Hu, H. X. Tang, G. E. Bauer, and Y. M. Blanter, *Phys. Rep.* **979**, 1 (2022).

[54] A. Blais, A. L. Grimsmo, S. M. Girvin, and A. Wallraff, *Rev. Mod. Phys.* **93**, 025005 (2021).

[55] D. Zoepfl, M. L. Juan, N. Diaz-Naufal, C. M. F. Schneider, L. F. Deeg, A. Sharafiev, A. Metelmann, and G. Kirchmair, *Phys. Rev. Lett.* **130**, 033601 (2023).

[56] Y.-P. Wang, G.-Q. Zhang, D. Zhang, X.-Q. Luo, W. Xiong, S.-P. Wang, T.-F. Li, C.-M. Hu, and J. Q. You, *Phys. Rev. B* **94**, 224410 (2016).

[57] Y.-P. Wang, G.-Q. Zhang, D. Zhang, T.-F. Li, C.-M. Hu, and J. Q. You, *Phys. Rev. Lett.* **120**, 057202 (2018).

[58] C. Gardiner and P. Zoller, *Quantum Noise: A Handbook of Markovian and Non-Markovian Quantum Stochastic Methods with Applications to Quantum Optics* (Springer, Berlin, Heidelberg, 2004).

[59] F. Quijandría, U. Naether, S. K. Özdemir, F. Nori, and D. Zueco, *Phys. Rev. A* **97**, 053846 (2018).

[60] A. Metelmann and A. A. Clerk, *Phys. Rev. X* **5**, 021025 (2015).

[61] S. Ghosh and T. C. H. Liew, *Phys. Rev. B* **97**, 241301 (2018).

[62] Y. Li, C. Wang, Y. Tang, and Y.-C. Liu, *Phys. Rev. Lett.* **132**, 183803 (2024).

[63] M. Harder, Y. Yang, B. M. Yao, C. H. Yu, J. W. Rao, Y. S. Gui, R. L. Stamps, and C.-M. Hu, *Phys. Rev. Lett.* **121**, 137203 (2018).

[64] J. M. P. Nair, D. Mukhopadhyay, and G. S. Agarwal, *Phys. Rev. B* **103**, 224401 (2021).

[65] C. Zhang, M. Kim, Y.-H. Zhang, Y.-P. Wang, D. Trivedi, A. Krasnok, J. Wang, D. Isleifson, R. Roshko, and C.-M. Hu, *APL Quantum* **2**, 011501 (2025).

[66] P. Z. G. Fonseca, E. B. Aranas, J. Millen, T. S. Monteiro, and P. F. Barker, *Phys. Rev. Lett.* **117**, 173602 (2016).

[67] Y. Tabuchi, S. Ishino, A. Noguchi, T. Ishikawa, R. Yamazaki, K. Usami, and Y. Nakamura, *Science* **349**, 405 (2015).

[68] S. P. Wolski, D. Lachance-Quirion, Y. Tabuchi, S. Kono, A. Noguchi, K. Usami, and Y. Nakamura, *Phys. Rev. Lett.* **125**, 117701 (2020).

[69] K. Fang, M. H. Matheny, X. Luan, and O. Painter, *Nat. Photonics* **10**, 489 (2016).

[70] J. G. E. Harris, H. Xu, L. Jiang, and D. Mason, *Nature (London)* **537**, 80 (2016).

[71] S. Forstner, S. Prams, J. Knittel, E. D. van Ooijen, J. D. Swaim, G. I. Harris, A. Szorkovszky, W. P. Bowen, and H. Rubinsztein-Dunlop, *Phys. Rev. Lett.* **108**, 120801 (2012).

[72] W. Xiong, Z. Li, Y. Song, J. Chen, G.-Q. Zhang, and M. Wang, *Phys. Rev. A* **104**, 063508 (2021).

[73] E. X. DeJesus and C. Kaufman, *Phys. Rev. A* **35**, 5288 (1987).